INTERNATIONAL JOURNAL OF
NUMERICAL ANALYSIS AND MODELING
Volume 18, Number 6, Pages 788–810

STABILITY ANALYSIS AND ERROR ESTIMATES OF LOCAL DISCONTINUOUS GALERKIN METHOD FOR CONVECTION-DIFFUSION EQUATIONS ON OVERLAPPING MESH WITH NON-PERIODIC BOUNDARY CONDITIONS

NATTAPORN CHUENJARERN, KANOGNUDGE WUTTANACHAMSRI, AND YANG YANG

Abstract. A new local discontinuous Galerkin (LDG) method for convection-diffusion equations on overlapping meshes with periodic boundary conditions was introduced in [14]. With the new method, the primary variable u and the auxiliary variable $p = u_x$ are solved on different meshes. In this paper, we will extend the idea to convection-diffusion equations with non-periodic boundary conditions, i.e. Neumann and Dirichlet boundary conditions. The main difference is to adjust the boundary cells. Moreover, we study the stability and suboptimal error estimates. Finally, numerical experiments are given to verify the theoretical findings.

Key words. Local discontinuous Galerkin method, stability, error analysis, overlapping meshes.

1. Introduction

In this paper, we apply the local discontinuous Galerkin (LDG) method on overlapping meshes provided in [14] for the convection-diffusion equations

$$u_t + f(u)_x = (a^2(u)u_x)_x, \quad x \in [0,1], \ t > 0, \tag{1}$$

as well as its two dimensional version. We assume that $a(u) \geq 0$.

In 1973, Reed and Hill first introduced the discontinuous Galerkin (DG) method in the framework of neutron linear transportation [23]. This method gained even greater popularity for good stability, high-order accuracy, and flexibility on h-p adaptivity and complex geometry. Subsequently, Cockburn et. al. proposed in a series of papers [6, 7, 8, 9] the Runge-Kutta discontinuous Galerkin (RKDG) methods for hyperbolic conservation laws. Later, in [10], Cockburn and Shu introduced the LDG method for convection-diffusion equations motivated by successfully solving compressible Navier-Stokes equations in [1].

As in traditional LDG method, we introduce an auxiliary variable $p = A(u)_x$ with $A(u) = \int^u a(s)\, ds$ to represent the derivative of the primary variable u, and rewrite (1) into the following system of first order equations

$$\begin{cases} u_t + f(u)_x = (a(u)p)_x, \\ p = A(u)_x. \end{cases} \tag{2}$$

Then we can solve u and p on the same mesh by using the DG method. The LDG method shares all the nice features of the DG methods for hyperbolic equations, and it becomes one of the most popular numerical methods for solving convection-diffusion equations. However, due to the discontinuity nature of the numerical approximations, it may not be easy to construct and analyze the scheme for some specials convection-diffusion equations. For example, the convection terms of chemotaxis model [19, 22] and miscible displacements in porous media [11, 12] are

Received by the editors April 9, 2020 and, in revised form, March 18, 2021.
2000 *Mathematics Subject Classification.* 65M12, 65M15, 65M20.

products of one of the primary variable and the derivative of another one. Therefore, the upwind flux for the convection term may not be easy to obtain. One of the alternatives is to use other methods, such as mixed finite element method, to obtain continuous approximations of the derivatives, see e.g. [18]. A more general idea is to use the Lax-Friedrichs flux, see e.g. [16, 20, 28] for the error estimates for miscible displacements and chemotaxis models. The main technique is to use the diffusion term to control the convection term [24, 25, 26]. Moreover, to make the numerical solutions to be physically relevant, we have to add a sufficiently large penalty which depends on the numerical approximations of the derivatives of the primary variables [17, 20, 2]. Another possible way is to construct flux-free schemes, such as the central discontinuous Galerkin (CDG) method [21] and the staggered discontinuous Galerkin (SDG) method [4]. However, the CDG scheme doubles the computational cost as we have to solve each equation in (2) on both the primary and dual meshes twice and it is not easy to apply limiters in SDG method because it requires partial continuity of the numerical approximations.

Recently, one of the authors in this paper introduced a new LDG method on overlapping meshes [14] by solving u and p on primitive and dual meshes, respectively, hence p is continuous across the interfaces on the primitive mesh. The scheme is proved to be stable under the L^2-norm and can be used to construct third-order maximum-principle-preserving schemes [13]. However, in some special cases, it may not enjoy the optimal convergence rates. The suboptimal convergence rate can be observed numerically if all the following three conditions are satisfied: (1) Odd order polynomials are used in the finite element space, (2) The dual mesh generated by connecting the midpoints of the primitive mesh, (3) No penalty is added to the numerical scheme. If one of the conditions is violated, the convergence rate will turn out to be optimal. Later, in [3], we used Fourier analysis to explicitly write out the error between the numerical and exact solutions and verify the optimal convergence rate for linear parabolic equations with periodic boundary conditions in one space dimension. Moreover, we also found out some superconvergence points that may depend on the perturbation constant in the construction of the dual mesh.

Both works given above are for problems with periodic boundary conditions. To implement the scheme, we need to combine the two boundary cells at the boundaries into one and find a polynomial approximation on the new cell. It is impossible to do that for general Dirichlet and Neumann boundary conditions, which are more realistic in practice, see e.g. [11, 12, 20]. In this paper, we will discuss the stability and error estimates of the new LDG methods for problems with Neumann and Dirichlet boundary conditions. The difficulty for the Neumann and Dirichlet boundary conditions is how to deal with the boundary cells of the dual mesh since two boundary cells cannot be combined. One possible way is to leave two boundary cells after generating the dual mesh, and introduce suitable numerical fluxes are the boundaries. For simplicity of presentation, we only demonstrate the proof for nonlinear parabolic equations

$$\begin{cases} u_t = (a(u)p)_x, \\ p = A(u)_x, \end{cases} \tag{3}$$

where $A(u) = \int^u a(t)\,dt$. The extension to general nonlinear convection-diffusion equations can be obtained following [14], hence we only demonstrate the results without proof.

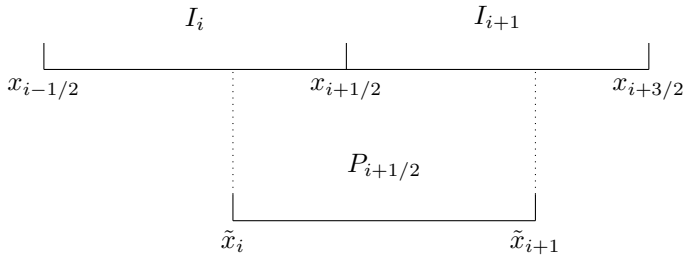

FIGURE 1. Overlapping meshes.

The rest of the paper is organized as follows: we first discuss the LDG scheme on overlapping mesh in Section 2. In Section 3, we demonstrate the stability analysis of the scheme for the Neumann and Dirichlet boundary conditions. The error estimate will be provided in Section 4. The extension to problems in two space dimensions will be discussed in Section 5. In Section 6, the numerical experiments will be given to demonstrate the accuracy of the scheme on non-periodic boundary conditions. We will end in Section 7 with concluding remarks.

2. Preliminary

In this section, we proceed to demonstrate the new LDG method for solving the one-dimensional diffusion equation (3) on overlapping meshes with three different boundary conditions, i.e. periodic, Neumann and Dirichlet boundary conditions.

2.1. Overlapping meshes. The new LDG method solves the variables u and p on two different meshes as shown in Figure 1. First, we define the primitive mesh on which the primary variable u is solved. We give a partition of the computational domain $\Omega = [0,1]$ as $0 = x_{\frac{1}{2}} < x_{\frac{3}{2}} < \cdots < x_{N+\frac{1}{2}} = 1$, and denote the $i-$th cell as

$$I_i = [x_{i-\frac{1}{2}}, x_{i+\frac{1}{2}}], \quad i = 1, ..., N.$$

Moreover, we denote

$$\Delta x_i = x_{i+\frac{1}{2}} - x_{i-\frac{1}{2}}, \quad x_i = \frac{x_{i+\frac{1}{2}} + x_{i-\frac{1}{2}}}{2}$$

as the cell length and the cell center of I_i, respectively, and define $\Delta x = \max_i \Delta x_i$.

We now demonstrate how to create the dual mesh, namely the P-mesh in [14], for solving the auxiliary variable p for problems with periodic boundary conditions. We choose a point $\tilde{x}_i$ given as

$$\tilde{x}_i = x_i + \frac{\Delta x_i}{2}\xi_{0,i}, \quad \xi_{0,i} \in [-1,1], \quad i = 1, ..., N. \tag{4}$$

It is easy to see that $\tilde{x}_i \in [x_{i-\frac{1}{2}}, x_{i+\frac{1}{2}}]$. Define

$$P_{i-\frac{1}{2}} = [\tilde{x}_{i-1}, \tilde{x}_i], \quad i = 1, ..., N,$$

as the $(i-\frac{1}{2})$-th cell of the dual mesh where we denote $\tilde{x}_0 = \tilde{x}_N - 1$. Moreover,

$$\Delta\tilde{x}_{i-\frac{1}{2}} = \tilde{x}_i - \tilde{x}_{i-1}, \quad \tilde{x}_{i-\frac{1}{2}} = \frac{\tilde{x}_i + \tilde{x}_{i-1}}{2}$$

stand for the cell length and the cell center of $P_{i-\frac{1}{2}}$, respectively. The P-mesh will consist of all P cells. For periodic boundary conditions, we can also define $P_{\frac{1}{2}} = [0, \tilde{x}_1] \cup [\tilde{x}_N, 1]$ as stated in [14], see Figure 2.

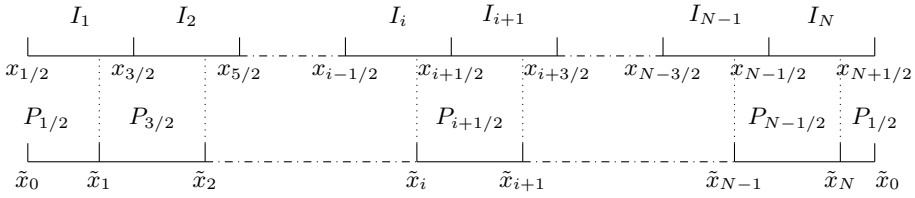

FIGURE 2. Overlapping meshes for periodic boundary conditions.

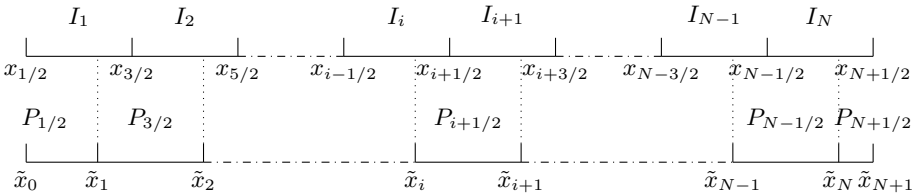

FIGURE 3. Overlapping mesh 1, L-mesh.

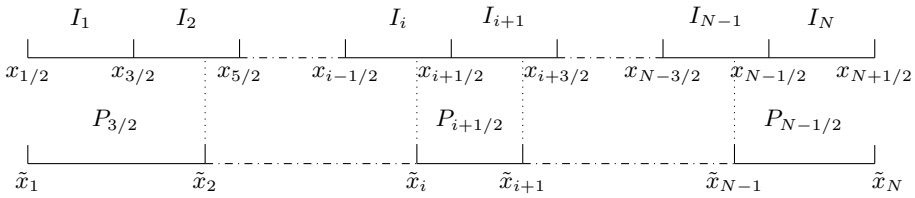

FIGURE 4. Overlapping mesh2, C-mesh.

Next, we demonstrate how to deal with the boundary cells on the P-mesh for problems with Neumann and Dirichlet boundary conditions. We leave the left and the right boundary cells and define $P_{\frac{1}{2}} = [0, \tilde{x}_1]$ and $P_{N+\frac{1}{2}} = [\tilde{x}_N, 1]$, see Figure 3. This mesh is called the L-mesh. The other way is to combine the boundary cells with their neighbour as $P_{\frac{3}{2}} = [0, \tilde{x}_2]$ and $P_{N-\frac{1}{2}} = [\tilde{x}_{N-1}, 1]$, see Figure 4. This mesh is called C-mesh.

If we take $\xi_{0,i}$ as a constant independent of i, it is easy to check that

$$\min\{\Delta x_{i-1}, \Delta x_i\} \le \Delta \tilde{x}_{i-\frac{1}{2}} \le \max\{\Delta x_{i-1}, \Delta x_i\},$$

and hence we have $\max_i \Delta \tilde{x}_{i-\frac{1}{2}} \le \Delta x$.

2.2. Norms. In this section, we define some norms that will be used throughout the paper.

For any interval I, we define $||u||_I$ and $||u||_{\infty,I}$ to be the standard L^2- and L^∞-norms of u on I, respectively. For any natural number ℓ, we consider the norm of Sobolev space $H^\ell(I)$, defined by

$$||u||_{\ell,I} = \left\{ \sum_{0\le\beta\le\ell} \left\| \frac{\partial^\beta u}{\partial x^\beta} \right\|_I^2 \right\}^{\frac{1}{2}}.$$

For convenience, if I is the whole computational domain, then the corresponding subscript will be omitted. Moreover, for any $u \in C(I_i)$, we define

$$||u||_{\Gamma_i} = |u^-_{i+\frac{1}{2}}| + |u^+_{i-\frac{1}{2}}|,$$

where Γ_i is the edges of the cell I_i. Similarly, for any $u \in C(P_{i-\frac{1}{2}})$, we define

$$||u||_{\Gamma_{i-\frac{1}{2}}} = |u_i^-| + |u_{i-1}^+|,$$

where $\Gamma_{i-\frac{1}{2}}$ is the edges of the cell $P_{i-\frac{1}{2}}$.

2.3. Numerical schemes with Neumann and Dirichlet boundary conditions. In this section, we consider the LDG method for the following nonlinear diffusion equation

$$\begin{cases} u_t = (a(u)p)_x, & x \in [0,1], \ t > 0, \\ p = A(u)_x, & x \in [0,1], \end{cases} \tag{5}$$

subject to the following boundary conditions

Neumann boundary condition:

$$u_x(0,t) = u_x(1,t) = 0. \tag{6}$$

Dirichlet boundary condition:

$$u(0,t) = u(1,t) = 0. \tag{7}$$

We define the finite element spaces to be

$$\begin{aligned} V_h &= \{u_h : u_h|_{I_i} \in P^k(I_i), i = 1, \dots, N\}, \\ P_h^L &= \{p_h : p_h|_{P_{i-\frac{1}{2}}} \in P^k(P_{i-\frac{1}{2}}), i = 1, \dots, N+1\}, \\ P_h^C &= \{p_h : p_h|_{P_{i-\frac{1}{2}}} \in P^k(P_{i-\frac{1}{2}}), i = 2, \dots, N\}, \end{aligned}$$

where P_h^L and P_h^C are finite element spaces for the L-mesh and C-mesh, respectively, and P^k is the space of polynomials of degree up to k.

Multiplying (5) with the test functions and using the integration by parts, we obtain

$$\int_{I_i} (u_h)_t v dx = -\int_{I_i} a(u_h) p_h v_x dx + \hat{a}_{i+\frac{1}{2}} \widehat{p_h}_{i+\frac{1}{2}} v_{i+\frac{1}{2}}^- - \hat{a}_{i-\frac{1}{2}} \widehat{p_h}_{i-\frac{1}{2}} v_{i-\frac{1}{2}}^+, \tag{8}$$

$$\int_{P_{i-\frac{1}{2}}} p_h w dx = -\int_{P_{i-\frac{1}{2}}} A(u_h) w_x dx + A(u_h(\tilde{x}_i)) w_i^- - A(u_h(\tilde{x}_{i-1})) w_{i-1}^+. \tag{9}$$

Then the LDG method on overlapping meshes is defined as follows:

- L-mesh: find $(u_h, p_h) \in V_h \times P_h^L$, such that for any test functions $(v, w) \in V_h \times P_h^L$ we have (8) and (9),
- C-mesh: find $(u_h, p_h) \in V_h \times P_h^C$, such that for any test functions $(v, w) \in V_h \times P_h^C$ we have (8) and (9),

where $v_{i+\frac{1}{2}}^- = v^-(x_{i+\frac{1}{2}})$ and $w_i^- = w^-(\tilde{x}_i)$. Likewise for $v_{i-\frac{1}{2}}^+$ and w_{i-1}^+.

We denote the jump of the function s across the cell interface $x = x_{i-\frac{1}{2}}$ as $[s]_{i-\frac{1}{2}} = s_{i-\frac{1}{2}}^+ - s_{i-\frac{1}{2}}^-$. Similarly, $[w]_i = w_i^+ - w_i^-$ denotes the jump of the function w across the cell interface $x = \tilde{x}_i$ on the P-mesh. The numerical flux $\hat{a}$ at the point $x_{i-\frac{1}{2}}$ is defined as

$$\hat{a}_{i-\frac{1}{2}} = \frac{[A(u_h)]_{i-\frac{1}{2}}}{[u_h]_{i-\frac{1}{2}}}. \tag{10}$$

Also, we choose the numerical flux $\widehat{p_h}_{i-\frac{1}{2}}$ as the value of p_h evaluated at $x = x_{i-\frac{1}{2}}$ with the penalty term

$$\widehat{p_h}_{i-\frac{1}{2}} = p_h(x_{i-\frac{1}{2}}) + \frac{\alpha_{i-\frac{1}{2}}}{\Delta\tilde{x}_{i-\frac{1}{2}}}[u_h]_{i-\frac{1}{2}}. \tag{11}$$

Notice that p_h is continuous at the interfaces of the primitive cells and hence $p_h(x_{i-\frac{1}{2}})$ is well defined. Due to the boundary conditions we also define the numerical fluxes of u and p on L-meshes as

Neumann boundary condition: $\widehat{p}_{\frac{1}{2}} = \widehat{p}_{N+\frac{1}{2}} = 0$.
Dirichlet boundary condition: $A(u_h(\tilde{x}_0)) = A(u_h(\tilde{x}_{N+1})) = A(0)$, ${u_h}^-_{\frac{1}{2}} = {u_h}^+_{N+\frac{1}{2}} = 0$.

The definition of the numerical fluxes at the boundary for C-mesh is similar.

Finally, we define

$$H_u(u_h, p_h, v) = -\sum_{i=1}^{N}\int_{I_i} a(u_h)p_h v_x dx + \sum_{i=1}^{N}\left(\hat{a}_{i+\frac{1}{2}}\hat{p}_{i+\frac{1}{2}}v^-_{i+\frac{1}{2}} - \hat{a}_{i-\frac{1}{2}}\hat{p}_{i-\frac{1}{2}}v^+_{i-\frac{1}{2}}\right), \tag{12}$$

$$H_p(u_h, w) = -\sum_{i=1}^{N+1}\int_{P_{i-\frac{1}{2}}} A(u_h)w_x dx + \sum_{i=1}^{N+1}\left(A(u_h(\tilde{x}_i))w_i^- - A(u_h(\tilde{x}_{i-1}))w_{i-1}^+\right), \tag{13}$$

for L-mesh. For C-mesh, the two summations in (13) are from $i = 2$ to N. Then the LDG scheme can be rewritten as

$$\int_\Omega (u_h)_t v dx = H_u(u_h, p_h, v), \tag{14}$$

$$\int_\Omega p_h w dx = H_p(u_h, w). \tag{15}$$

3. Stability analysis

In this section, we demonstrate the stability of the new LDG method on overlapping meshes with non-periodic boundary conditions.

3.1. Neumann boundary condition.

In this subsection, the stability of the new LDG method on overlapping meshes with the Neumann boundary conditions will be demonstrated.

Lemma 3.1. *Suppose H_u and H_p are defined in* (12) *and* (13)*, respectively, and the dual mesh is given as either the L-mesh or the C-mesh, then we have*

$$H_u(u_h, p_h, u_h) + H_p(u_h, p_h) = -\sum_{i=2}^{N}\frac{[A(u_h)]_{i-\frac{1}{2}}}{[u_h]_{i-\frac{1}{2}}}\frac{\alpha_{i-\frac{1}{2}}}{\Delta\tilde{x}_{i-\frac{1}{2}}}[u_h]^2_{i-\frac{1}{2}}. \tag{16}$$

Proof. We only prove for L-mesh. The case for C-mesh is basically the same. Taking $w = p_h$ in (13), using integration by parts and applying the Neumann boundary

conditions, we obtain

$$\begin{aligned}
H_p(u_h,p_h) &= -\sum_{i=1}^{N+1}\int_{P_{i-\frac{1}{2}}} A(u_h)(p_h)_x dx \\
&\quad + \sum_{i=1}^{N+1}\left(A(u_h(\tilde{x}_i))(p_h^-)_i - A(u_h(\tilde{x}_{i-1}))(p_h^+)_{i-1}\right) \\
&= -\int_{P_{\frac{1}{2}}} A(u_h)(p_h)_x dx + A(u_h(\tilde{x}_1))(p_h^-)_1 - A(u_h(\tilde{x}_0))(p_h^+)_0 \\
&\quad - \sum_{i=2}^{N}\int_{\tilde{x}_{i-1}}^{x_{i-\frac{1}{2}}} A(u_h)(p_h)_x dx - \sum_{i=2}^{N}\int_{x_{i-\frac{1}{2}}}^{\tilde{x}_i} A(u_h)(p_h)_x dx \\
&\quad + \sum_{i=2}^{N}\left(A(u_h(\tilde{x}_i))(p_h^-)_i - A(u_h(\tilde{x}_{i-1}))(p_h^+)_{i-1}\right) \\
&\quad - \int_{P_{N+\frac{1}{2}}} A(u_h)(p_h)_x dx + A(u_h(\tilde{x}_{N+1}))(p_h^-)_{N+1} - A(u_h(\tilde{x}_N))(p_h^+)_N \\
&= \int_{P_{\frac{1}{2}}} a(u_h)(u_h)_x p_h dx \\
&\quad + \sum_{i=2}^{N}\int_{\tilde{x}_{i-1}}^{x_{i-\frac{1}{2}}} a(u_h)(u_h)_x p_h dx + \sum_{i=2}^{N}\int_{x_{i-\frac{1}{2}}}^{\tilde{x}_i} a(u_h)(u_h)_x p_h dx \\
&\quad + \sum_{i=2}^{N}[A(u_h)]_{i-\frac{1}{2}} p_h(x_{i-\frac{1}{2}}) + \int_{P_{N+\frac{1}{2}}} a(u_h)(u_h)_x p_h dx \\
&= \sum_{i=1}^{N}\int_{I_i} a(u_h)(u_h)_x p_h dx + \sum_{i=2}^{N}[A(u_h)]_{i-\frac{1}{2}} p_h(x_{i-\frac{1}{2}}). \qquad (17)
\end{aligned}$$

Taking $v = u_h$ in (12), we obtain

$$\begin{aligned}
H_u(u_h,p_h,v) &= -\sum_{i=1}^{N}\int_{I_i} p_h a(u_h)(u_h)_x dx - \sum_{i=2}^{N}\hat{a}_{i-\frac{1}{2}}\hat{p}_{i-\frac{1}{2}}[u_h]_{i-\frac{1}{2}} \\
&\quad - \hat{a}_{\frac{1}{2}}\hat{p}_{\frac{1}{2}}(u_h)^+_{\frac{1}{2}} + \hat{a}_{N+\frac{1}{2}}\hat{p}_{N+\frac{1}{2}}(u_h)^-_{N+\frac{1}{2}} \\
&= -\sum_{i=1}^{N}\int_{I_i} p_h a(u_h)(u_h)_x dx \\
&\quad - \sum_{i=2}^{N}\frac{[A(u_h)]_{i-\frac{1}{2}}}{[u_h]_{i-\frac{1}{2}}}\left(p_h(x_{i-\frac{1}{2}}) + \frac{\alpha_{i-\frac{1}{2}}}{\Delta\tilde{x}_{i-\frac{1}{2}}}\right)[u_h]_{i-\frac{1}{2}}. \qquad (18)
\end{aligned}$$

where the last step, we obtain it by applying the Neumann boundary conditions. Summing (17) and (18), we have (16) which further leads to the L^2 stability of the LDG method on overlapping meshes with Neumann boundary conditions. □

3.2. Dirichlet boundary conditions. In this subsection, we will describe the stability of the new LDG method on overlapping meshes for problems with Dirichlet boundary conditions.

With a minor change of the previous proof, we can obtain the following lemma.

Lemma 3.2. *Suppose H_u and H_p defined in* (12) *and* (13)*, respectively, then we have*

$$H_u(u_h, p_h, u_h) + H_p(u_h, p_h) = -\sum_{i=1}^{N+1} \frac{[A(u_h)]_{i-\frac{1}{2}}}{[u_h]_{i-\frac{1}{2}}} \frac{\alpha_{i-\frac{1}{2}}[u_h]^2_{i-\frac{1}{2}}}{\Delta\tilde{x}_{i-\frac{1}{2}}}. \tag{19}$$

The proof is very similar to that of Lemma 3.1, so we omit it and only demonstrate the result as the following theorem.

Theorem 3.3. *The LDG method introduced* (8) *and* (9) *with the boundary conditions* (6) *and* (7) *are stable and*

$$\frac{1}{2}\frac{d}{dt}||u_h||^2 + ||p_h||^2 \leq 0.$$

4. Error estimates

In this section, we demonstrate the error estimates. We will consider linear equations. Moreover, for simplicity, we will discuss the problem with the Neumann boundary condition on L-meshes only. For the other cases, we can apply the same procedure.

First, we use e to denote the error between the exact and numerical solutions i.e. $e_u = u - u_h$ and $e_p = p - p_h$, then we can get the error equations from (8) and (9) as

$$\int_{I_i} (e_u)_t v dx = -\int_{I_i} e_p v_x dx + \widehat{e_p}_{i+\frac{1}{2}} v^-_{i+\frac{1}{2}} - \widehat{e_p}_{i-\frac{1}{2}} v^+_{i-\frac{1}{2}}, \tag{20}$$

$$\int_{P_{i-\frac{1}{2}}} e_p w dx = -\int_{P_{i-\frac{1}{2}}} e_u w_x dx + e_u(\tilde{x}_i) w^-_i - e_u(\tilde{x}_{i-1}) w^+_{i-1}. \tag{21}$$

Next, we introduce some basic properties of the finite element space that will be used.

Lemma 4.1. *Assuming $u \in V_h$, there exists constant $C > 0$ independent of Δx and u such that for $\beta \geq 1$*

$$||\partial_x^\beta u||_{I_i} \leq C\Delta x_i^{-\beta}||u||_{I_i}, \quad ||u||_{\Gamma_i} \leq C\Delta x_i^{-1/2}||u||_{I_i}.$$

Similarly, for any $u \in P_h^L$, there exists constant $C > 0$ independent of $\Delta\tilde{x}$ and u such that for $\beta \geq 1$

$$||\partial_x^\beta u||_{P_{i-\frac{1}{2}}} \leq C\Delta\tilde{x}_{i-\frac{1}{2}}^{-\beta}||u||_{P_{i-\frac{1}{2}}}, \quad ||u||_{\Gamma_{i-\frac{1}{2}}} \leq C\Delta\tilde{x}_{i-\frac{1}{2}}^{-1/2}||u||_{P_{i-\frac{1}{2}}}.$$

We also introduce the standard L^2 projections P_k^1 into V_h and P_k^2 into P_h^L by:

$$\int_{I_i} P_k^1 uv dx = \int_{I_i} uv dx, \ \forall v \in P^k(I_i),$$

and

$$\int_{P_{i-\frac{1}{2}}} P_k^2 uv dx = \int_{P_{i-\frac{1}{2}}} uv dx, \ \forall v \in P^k(P_{i-\frac{1}{2}}),$$

respectively. By the scaling argument, we obtain the following lemma [5]

Lemma 4.2. *Suppose the function $u(x) \in C^{k+1}(I_i)$, then there exists positive constant C independent of Δx and u, such that*

$$||u - P_k^1 u||_{I_i} + \Delta x_i||(u - P_k^1 u)_x||_{I_i} + \Delta x_i^{1/2}||u - P_k^1 u||_{\infty, I_i} \leq C\Delta x_i^{k+1}||u||_{k+1, I_i}.$$

Moreover, if $u(x) \in C^{k+1}(P_{i-\frac{1}{2}})$, then there exists positive constant C independent of $\Delta\tilde{x}$ and u, such that

$$\begin{aligned}&||u - P_k^2 u||_{P_{i-\frac{1}{2}}} + \Delta\tilde{x}_{i-\frac{1}{2}}||(u - P_k^2 u)_x||_{P_{i-\frac{1}{2}}} + \Delta\tilde{x}_{i-\frac{1}{2}}^{1/2}||u - P_k^2 u||_{\infty, P_{i-\frac{1}{2}}}\\ \leq& C\Delta\tilde{x}_{i-\frac{1}{2}}^{k+1}||u||_{k+1, P_{i-\frac{1}{2}}},\end{aligned}$$

where $||u||_{k+1,I}$ is the standard H^{k+1}-norm over the interval I.

As the general treatment of the finite element method, we split the errors into two terms as

$$e_u = \eta_u - \xi_u, \quad e_p = \eta_p - \xi_p,$$

where

$$\eta_u = u - P_k^1 u, \quad \xi_u = u_h - P_k^1 u, \quad \eta_p = p - P_k^2 p, \quad \xi_p = p_h - P_k^2 p.$$

With the above notations, the equations (20) and (21) can be rewritten as

$$\int_{I_i} (\xi_u)_t v dx = \int_{I_i} e_p v_x dx - \widehat{e_p}_{i+\frac{1}{2}} v_{i+\frac{1}{2}}^+ - \widehat{e_p}_{i-\frac{1}{2}} v_{i-\frac{1}{2}}^+ \tag{22}$$

$$\int_{P_{i-\frac{1}{2}}} \xi_p w dx = \int_{P_{i-\frac{1}{2}}} e_u w_x dx - e_u(\tilde{x}_i) w_i^- + e_u(\tilde{x}_{i-1}) w_{i-1}^+ \tag{23}$$

Now, we can state the main theorem.

Theorem 4.3. *Suppose the exact solution $u \in C^{k+2}(\Omega)$ and the finite element space is made up of piecewise polynomials of degree k. Moreover, the numerical solutions satisfy* (8) *and* (9)*. Then the error between the numerical and exact solutions satisfies*

$$||e_u|| + \int_0^T ||e_p|| dt \leq C\Delta x^k,$$

where C is independent of Δx.

Proof. Sum up (22) and (23) with $v = \xi_u$ and $w = \xi_p$, and then sum up over i to obtain

$$\begin{aligned}&\frac{1}{2}\frac{d}{dt}||\xi_u||^2 + ||\xi_p||^2\\ =& \sum_{i=1}^N \int_{I_i} (\eta_p - \xi_p)(\xi_u)_x dx + \sum_{i=2}^N \left(\eta_{p_{i-\frac{1}{2}}} - \xi_{p_{i-\frac{1}{2}}} + \alpha_{i-\frac{1}{2}} \frac{[\eta_u - \xi_u]_{i-\frac{1}{2}}}{\Delta\tilde{x}_{i-\frac{1}{2}}}\right)[\xi_u]_{i-\frac{1}{2}}\\ &- \sum_{i=1}^N \int_{I_i} (\eta_u - \xi_u)(\xi_p)_x dx - \sum_{i=2}^N [\eta_u - \xi_u]_{i-\frac{1}{2}} \xi_p(x_{i-\frac{1}{2}})\\ =& \sum_{i=1}^N \int_{I_i} \eta_p(\xi_u)_x dx + \sum_{i=2}^N \left(\eta_{p_{i-\frac{1}{2}}} + \alpha_{i-\frac{1}{2}} \frac{[\eta_u]_{i-\frac{1}{2}}}{\Delta\tilde{x}_{i-\frac{1}{2}}}\right)[\xi_u]_{i-\frac{1}{2}}\\ &- \sum_{i=1}^N \int_{I_i} \eta_u(\xi_p)_x dx - \sum_{i=2}^N [\eta_u]_{i-\frac{1}{2}} \xi_p(x_{i-\frac{1}{2}}) + H_u^N(\xi_u, \xi_p, \xi_u) + H_p^N(\xi_u, \xi_p)\\ =& R_1 + R_2 + R_3,\end{aligned} \tag{24}$$

where

$$R_1 = \sum_{i=1}^{N} \int_{I_i} \eta_p (\xi_u)_x dx - \sum_{i=1}^{N} \int_{I_i} \eta_u (\xi_p)_x dx,$$
$$R_2 = \sum_{i=2}^{N} \left(\alpha_{i-\frac{1}{2}} \frac{[\eta_u]_{i-\frac{1}{2}}}{\Delta \tilde{x}_{i-\frac{1}{2}}} \right) [\xi_u]_{i-\frac{1}{2}} + H_u^N(\xi_u, \xi_p, \xi_u) + H_p^N(\xi_u, \xi_p),$$
$$R_3 = \sum_{i=2}^{N} \eta_{p_{i-\frac{1}{2}}} [\xi_u]_{i-\frac{1}{2}} - \sum_{i=2}^{N} [\eta_u]_{i-\frac{1}{2}} \xi_p(x_{i-\frac{1}{2}}).$$

Now we estimate R_i where $i = 1, 2, 3$ term by term.

$$\begin{aligned} R_1 &\le \sum_{i=1}^{N} (||\eta_p||_{I_i} ||(\xi_u)_x||_{I_i} + ||(\eta_u)_x||_{I_i} ||\xi_p||_{I_i}) \\ &\le \sum_{i=1}^{N} \left(||\eta_p||_{P_{i-\frac{1}{2}} \cup P_{i+\frac{1}{2}}} ||\xi_u||_{I_i} + ||(\eta_u)_x||_{I_i} ||\xi_p||_{I_i} \right) \\ &\le C\Delta x^k \sum_{i=1}^{N} \left[\left(||p||_{k+1, P_{i-\frac{1}{2}}} + ||p||_{k+1, P_{i+\frac{1}{2}}} \right) ||\xi_u||_{I_i} + ||u||_{k+1, I_i} ||\xi_p||_{I_i} \right] \\ &\le C\Delta x^k \left(||\xi_u|| + ||\xi_p|| \right), \end{aligned} \tag{25}$$

where we applied the Cauchy-Schwarz inequality to the first step. In the second step, we used Lemmas 4.1 and 4.2. Also, the Cauchy-Schwarz inequality was used again in the last step. Applying Lemma 3.1, we obtain the estimate of R_2

$$\begin{aligned} R_2 &\le \sum_{i=2}^{N} \frac{\alpha_{i-\frac{1}{2}}}{\Delta \tilde{x}_{i-\frac{1}{2}}} \left([\eta_u]_{i-\frac{1}{2}} [\xi_u]_{i-\frac{1}{2}} - [\xi_u]_{i-\frac{1}{2}}^2 \right) \\ &\le C \sum_{i=2}^{N} \frac{\alpha_{i-\frac{1}{2}}}{\Delta x} [\eta_u]_{i-\frac{1}{2}}^2 \\ &\le C \sum_{i=2}^{N} \alpha_{i-\frac{1}{2}} \Delta x^{2k} \left(||u||_{I_{i-1}}^2 + ||u||_{I_i}^2 \right) \\ &\le C\Delta x^{2k}, \end{aligned} \tag{26}$$

where Lemma 4.2 was applied in step 2. While steps 2 and 4 follow from direct computation. Finally, we estimate R_3.

$$\begin{aligned} R_3 &\le \sum_{i=2}^{N} ||\eta_p||_{\infty, P_{i-\frac{1}{2}}} \left(||\xi_u||_{\Gamma_{i-1}} + ||\xi_u||_{\Gamma_i} \right) + \sum_{i=2}^{N} \left(||\eta_u||_{\Gamma_{i-1}} + ||\eta_u||_{\Gamma_i} \right) ||\xi_p||_{\infty, I_i} \\ &\le C\Delta x^k \sum_{i=2}^{N} \left[||p||_{k+1, P_{i-\frac{1}{2}}} \left(||\xi_u||_{i-1} + ||\xi_u||_i \right) + \left(||u||_{i-1} + ||u||_i \right) ||\xi_p||_{k+1, I_i} \right] \\ &\le C\Delta x^k \left(||p||_{k+1} ||\xi_u|| + ||u||_{k+1} ||\xi_p|| \right), \end{aligned} \tag{27}$$

where step 1 is straightforward, step 2 follows from Lemmas 4.1 and 4.2 and the last step we applied the Cauchy-Schwarz inequality. Substitute (25)-(27) into (24) to obtain

$$\frac{1}{2} \frac{d}{dt} ||\xi_u||^2 + ||\xi_p||^2 \le C\Delta x^{2k} + C\Delta x^k (||\xi_u|| + ||\xi_p||),$$

which further yields

$$\frac{1}{2}\frac{d}{dt}||\xi_u||^2 + ||\xi_p||^2 \leq C\Delta x^{2k} + ||\xi_u||^2.$$

Finally, we can apply the Gronwall's inequality and complete the proof. □

5. Numerical scheme for two-dimensional case

In this section, we will construct the scheme in two-dimensional case for the following problem over the domain $\Omega = [0,1] \times [0,1]$

$$\begin{cases} u_t = (a(u)p)_x + (b(u)q)_x, \\ p = A(u)_x, \\ q = B(u)_y, \end{cases} \tag{28}$$

where $A(u) = \int^u a(t)dt$ and $B(u) = \int^u b(t)dt$. We consider the following boundary conditions

Neumann boundary condition:

$$u_x(0,y,t) = u_x(1,y,t) = u_y(x,0,t) = u_y(x,1,t) = 0. \tag{29}$$

Dirichlet boundary condition:

$$u(0,y,t) = u(1,y,t) = u(x,0,t) = u(x,1,t) = 0. \tag{30}$$

First, we give a rectangular decomposition of Ω which is the primitive mesh for the primary variable u. Let $0 = x_{\frac{1}{2}} < x_{\frac{3}{2}} < \cdots < x_{N_x+\frac{1}{2}} = 1$, and $0 = y_{\frac{1}{2}} < y_{\frac{3}{2}} < \cdots < y_{N_y+\frac{1}{2}} = 1$ be grid points in x and y directions, respectively, and denote the $i,j-th$ cell as

$$I_{ij} = I_i \times J_j = [x_{i-\frac{1}{2}}, x_{i+\frac{1}{2}}] \times [y_{j-\frac{1}{2}}, y_{j+\frac{1}{2}}]$$

for all $i = 1,\ldots,N_x$ and $j = 1,\ldots,N_y$. Also, we denote

$$\Delta x_i = x_{i+\frac{1}{2}} - x_{i-\frac{1}{2}}, \quad x_i = \frac{x_{i+\frac{1}{2}} + x_{i-\frac{1}{2}}}{2}, \quad \Delta y_i = y_{j+\frac{1}{2}} - y_{j-\frac{1}{2}}, \quad y_j = \frac{y_{j+\frac{1}{2}} + y_{j-\frac{1}{2}}}{2},$$

and

$$\Delta x = \max_i \Delta x_i, \quad \Delta y = \max_j \Delta y_j, \quad h = \max\{\Delta x, \Delta y\}.$$

Next, we define the P-mesh and Q-mesh for solving the auxiliary variable p and q. We choose $\tilde{x}_i$ given as

$$\tilde{x}_i = x_i + \frac{\Delta x_i}{2}\xi_0, \quad \xi_0 \in [-1,1] \tag{31}$$

to define the P-mesh as

$$P_{i-\frac{1}{2},j} = [\tilde{x}_{i-1}, \tilde{x}_i] \times [y_{j-\frac{1}{2}}, y_{j+\frac{1}{2}}], \quad i = 1,...,N_x,$$

with $\tilde{x}_0 = \tilde{x}_{N_x-1}$. Similarly, we pick a point $\tilde{y}_j$ given as

$$\tilde{y}_j = y_j + \frac{\Delta y_j}{2}\eta_0, \quad \eta_0 \in [-1,1], \tag{32}$$

and define Q-mesh as

$$Q_{i,j-\frac{1}{2}} = [x_{i-\frac{1}{2}}, x_{i+\frac{1}{2}}] \times [\tilde{y}_{j-1}, \tilde{y}_j], \quad j = 1,...,N_y,$$

with $\tilde{y}_0 = \tilde{y}_{N_y-1}$. Similar to the problem in one space dimension, we need to deal with the boundary cells for problems with the Neumann and Dirichlet boundary conditions. We can leave the left and right boundary cells as $P_{\frac{1}{2},j} = [0,\tilde{x}_1] \times J_j$, $P_{N_x+\frac{1}{2},j} = [\tilde{x}_{N_x},1] \times J_j$, $Q_{i,\frac{1}{2}} = I_i \times [0,\tilde{y}_1]$ and $Q_{i,N_y+\frac{1}{2}} = I_i \times [\tilde{y}_{N_y},1]$. This mesh

is called the L-mesh. The other way is to combine the boundary cells with their neighbour as $P_{\frac{3}{2},j} = [0, \tilde{x}_2] \times J_j, P_{N_x-\frac{1}{2}} = [\tilde{x}_{N_x-1}, 1] \times J_j, Q_{i,\frac{3}{2}} = I_i \times [0, \tilde{x}_2]$ and $Q_{N_y-\frac{1}{2}} = I_i \times [\tilde{y}_{N_y-1}, 1]$. This mesh is called C-mesh.

We define the finite element spaces for the L-mesh, P_h^L and Q_h^L, and for the C-mesh, P_h^C and Q_h^C, to be

$$
\begin{aligned}
V_h &= \{u_h : u_h|_{I_ij} \in P^k(I_ij), i = 1, \ldots, N_x, j = 1, \ldots, N_y\},\\
P_h^L &= \{p_h : p_h|_{P_{i-\frac{1}{2},j}} \in P^k(P_{i-\frac{1}{2},j}), i = 1, \ldots, N_x + 1, j = 1, \ldots, N_y\},\\
P_h^C &= \{p_h : p_h|_{P_{i-\frac{1}{2},j}} \in P^k(P_{i-\frac{1}{2},j}), i = 2, \ldots, N_x, j = 1, \ldots, N_y\},\\
Q_h^L &= \{p_h : p_h|_{Q_{i,j-\frac{1}{2}}} \in P^k(Q_{i,j-\frac{1}{2}}), i = 1, \ldots, N_x, j = 2, \ldots, N_y + 1\},\\
Q_h^C &= \{p_h : p_h|_{Q_{i,j-\frac{1}{2}}} \in P^k(Q_{i,j-\frac{1}{2}}), i = 1, \ldots, N_x, j = 2, \ldots, N_y\},
\end{aligned}
$$

where P^k is the space of polynomials of degree up to k.

Now, we can introduce the LDG method on overlapping mesh for (28). Multiplying the test functions and using the integration by parts, we obtain

$$
\begin{aligned}
\int_{I_{ij}} (u_h)_t v dx dy = &- \int_{I_i} a(u_h) p_h v_x dx dy + \int_{J_j} \hat{a}_{i+\frac{1}{2},j} \widehat{p_h}_{i+\frac{1}{2},j} v^-_{i+\frac{1}{2},j} dy\\
&- \int_{J_j} \hat{a}_{i-\frac{1}{2},j} \widehat{p_h}_{i-\frac{1}{2},j} v^+_{i-\frac{1}{2},j} dy - \int_{J_i} b(u_h) p_h v_y dx dy\\
&+ \int_{I_i} \hat{a}_{i,j+\frac{1}{2}} \widehat{p_h}_{i,j+\frac{1}{2}} v^-_{i,j+\frac{1}{2}} dx - \int_{I_i} \hat{a}_{i,j-\frac{1}{2}} \widehat{p_h}_{i,j-\frac{1}{2}} v^+_{i,j-\frac{1}{2}} dx, \qquad (33)
\end{aligned}
$$

$$
\begin{aligned}
\int_{P_{i-\frac{1}{2},j}} p_h w dx d = &- \int_{P_{i-\frac{1}{2},j}} A(u_h) w_x dx dy + \int_{J_j} A(u_h(\tilde{x}_i)) w_i^- dy\\
&- \int_{J_j} A(u_h(\tilde{x}_{i-1})) w^+_{i-1} dy, \qquad (34)
\end{aligned}
$$

$$
\begin{aligned}
\int_{Q_{i,j-\frac{1}{2}}} q_h z dx dy = &- \int_{Q_{i,j-\frac{1}{2}}} B(u_h) z_y dx dy + \int_{I_i} B(u_h(\tilde{y}_j)) z_j^- dx\\
&- \int_{I_i} B(u_h(\tilde{y}_{j-1})) z^+_{j-1} dx. \qquad (35)
\end{aligned}
$$

Then the LDG method on overlapping meshes for (28) is defined as follows:

- L-mesh: find $(u_h, p_h, q_h) \in V_h \times P_h^L \times Q_h^L$, such that for any test functions $(v, w, z) \in V_h \times P_h^L \times Q_h^L$ we have (33) - (35),
- C-mesh: find $(u_h, p_h, q_h) \in V_h \times P_h^C \times Q_h^C$, such that for any test functions $(v, w, z) \in V_h \times P_h^C \times Q_h^C$ we have (33) - (35).

We denoted $u^+_{i-\frac{1}{2},j}, u^-_{i+\frac{1}{2},j}, u^+_{i,j-\frac{1}{2}}, u^+_{i,j+\frac{1}{2}}$ as the traces of $u \in V_h$ on the four edges of I_{ij}, respectively. Likewise for the traces of along the vertical edges of $P_{i-\frac{1}{2},j}$ and the horizontal edges of $Q_{i,j-\frac{1}{2}}$. Moreover, we use $[u] = u^+ - u^-$ and $\{u\} = \dfrac{1}{2}(u^+ + u^-)$ as the jump and average of u at the cells interfaces, receptively. Due to the boundary conditions we also define the numerical fluxes of u and p on L-meshes as

Neumann boundary condition: $\widehat{p}_{i,\frac{1}{2}} = \widehat{p}_{i,N+\frac{1}{2}} = 0$, and $\widehat{p}_{\frac{1}{2},j} = \widehat{p}_{N+\frac{1}{2},j} = 0$.
Dirichlet boundary condition: $A(u_h(\tilde{x}_{i,0})) = A(u_h(\tilde{x}_{i,N+1})) = A(0)$, ${u_h}^-_{i,\frac{1}{2}} = {u_h}^+_{i,N+\frac{1}{2}} = 0$ and $A(u_h(\tilde{x}_{0,j})) = A(u_h(\tilde{x}_{N+1,j})) = A(0)$, ${u_h}^-_{\frac{1}{2},j} = {u_h}^+_{N+\frac{1}{2},j} = 0$.

The definition of the numerical fluxes at the boundary for C-mesh is similar.

The numerical flux $\hat{a}$ along the edge $x_{i-\frac{1}{2}}$ is defined as

$$\hat{a}_{i-\frac{1}{2},j} = \frac{[A(u_h)]_{i-\frac{1}{2},j}}{[u_h]_{i-\frac{1}{2}},j}. \tag{36}$$

Similarly, the numerical flux $\hat{b}$ along the edge $y_{j-\frac{1}{2}}$ is defined as

$$\hat{b}_{j-\frac{1}{2}} = \frac{[B(u_h)]_{i,j-\frac{1}{2}}}{[u_h]_{i,j-\frac{1}{2}}}. \tag{37}$$

Also, we choose the numerical flux

$$\widehat{p_h}_{i-\frac{1}{2},j} = p_h(x_{i-\frac{1}{2}}, y) + \frac{\alpha_{i-\frac{1}{2},j}}{\Delta\tilde{x}_{i-\frac{1}{2},j}}[u_h]_{i-\frac{1}{2},j}, \tag{38}$$

and

$$\widehat{q_h}_{i,j-\frac{1}{2}} = q_h(x, y_{j-\frac{1}{2}}) + \frac{\alpha_{i,j-\frac{1}{2}}}{\Delta\tilde{y}_{i,j-\frac{1}{2},j}}[u_h]_{i,j-\frac{1}{2}}, \tag{39}$$

where $[s]_{i-\frac{1}{2},j} = s^+_{i-\frac{1}{2},j} - s^-_{i-\frac{1}{2},j}$ stands for the jump of the function s across the cell boundary $\{x_{i-\frac{1}{2}}\} \times J_j$. Similarly for $[s]_{i,j-\frac{1}{2}}$.

To obtain the stability analysis and error estimates, we can follow the same analyses for the problem in one-dimensional space. Therefore, we will omit the proof and only state the results in the following two theorems.

Theorem 5.1. *The LDG method introduced* (33), (34) *and* (35) *with the boundary conditions* (29) *and* (30) *are stable and*

$$\frac{1}{2}\frac{d}{dt}||u_h||^2 + ||p_h||^2 + ||q_h||^2 \leq 0.$$

Theorem 5.2. *Suppose the exact solution for linear parabolic equation* (28) *with* $a(u) = b(u) = 1$ *satisfies* $u \in C^{k+1}(\Omega)$ *and the finite element space is made up of piecewise polynomial of degree* k *in each cell. The numerical solutions satisfy* (33) - (35). *Then the error between the numerical and exact solutions satisfies*

$$||u - u_h|| + \int_0^T ||p - p_h|| + ||q - q_h||dt \leq Ch^k,$$

where C *is independent of* h.

6. Numerical Experiments

In this section, several numerical experiments will be given to demonstrate the stability and accuracy of the new LDG method on overlapping mesh for non-periodic boundary conditions.

6.1. Parabolic equations. In this subsection, we will discuss pure parabolic equations only.

Example 6.1. *To compare the CFL number for two different meshes, we consider third-order SSP Runge-Kutta time discretization* [15] *to solve the following heat equation in one space dimension*

$$u_t = u_{xx}, \quad x \in [0, 2\pi], \tag{40}$$

TABLE 1. Example 6.1: The results of CFL testing.

CFL	N	L-mesh				C-mesh			
		Neumann		Dirichlet		Neumann		Dirichlet	
		L^2 norm	order	L^2 norm	order	L^2 norm	order	L^2 norm	order
0.25	10	1.65E-01	-	9.22E+00	-	4.68E-02	-	6.47E-02	-
	20	1.37E+01	-	1.45E+07	-	1.83E-02	1.36	2.36E-02	1.46
	40	2.06E+12	-	2.27E+33	-	8.48E-03	1.11	9.70E-03	1.28
	80	1.17E+59	-	1.31E+143	-	4.23E-03	1.00	4.52E-03	1.10
	160	INF	-	Nan	-	2.12E-03	0.99	2.19E-03	1.05

subject to Neumann and Dirichlet boundary conditions

$$u_x(0,t) = u_x(2\pi,t) = 0,$$
$$u(0,t) = u(2\pi,t) = 0,$$

respectively.

We consider a uniform mesh and use linear polynomial P^1 with the dual mesh is generated by using the midpoint of the primitive mesh to compare the CFL number to the two different meshes. The results in Table 1 shows that the CFL number for C-mesh is larger than that for L-mesh. This is mainly because the small cell effect does not works for C-mesh as we combine the small cells near the boundary with its neighbor. For all the following numerical experiments, we use piecewise polynomials of degree $k = 1, 2$. Moreover, we consider third-order SSP Runge-Kutta time discretization [15] with $\Delta t = 0.01\Delta x^2$ to reduce the time error.

Example 6.2. *We solve the following heat equation in one space dimension*

$$\begin{cases} u_t = u_{xx}, \quad x \in [0, 2\pi], \\ u(x,0) = \cos(x), \end{cases} \tag{41}$$

with Neumann boundary condition

$$u_x(0,t) = u_x(2\pi,t) = 0. \tag{42}$$

Clearly, the exact solution is

$$u(x,t) = e^{-t}\cos(x).$$

We consider a uniform mesh and take $\xi_0 = 0$ in (4), i.e. the dual mesh is generated by using the midpoint of the primitive mesh. We take the final time $T = 0.5$ and compute the L^2-norm of the error between the numerical and exact solutions. In Table 2, the results show that we can only obtain suboptimal accuracy if k is an odd number with the penalty parameter $\alpha = 0$. One way to obtain the optimal accuracy is to choose $\alpha \neq 0$.

In addition, we also take $\alpha = 0$ and $\xi_0 = 0.1$ which is closed to 0 and $\xi_0 = \sqrt{3}/3$ which is away from 0. The results in Table 3 demonstrated that we may recover the optimal convergence rates if we take $\xi_0 \neq 0$. However, we may observe only the $k + \dfrac{1}{2}$ order of accuracy when we consider the C-mesh treatment without the penalty term.

Example 6.3. *We solve*

$$\begin{cases} u_t = u_{xx}, \quad x \in [0, 2\pi], \\ u(x,0) = \sin(x), \end{cases} \tag{43}$$

TABLE 2. Example 6.2: midpoint with Neumann boundary condition.

k	N	L-mesh				C-mesh			
		no penalty		$\alpha = 1.0$		no penalty		$\alpha = 1.0$	
		L^2 norm	order	L^2 norm	order	L^2 norm	order	L^2 norm	order
1	10	9.51E-02	-	2.12E-02	-	3.91E-02	-	2.78E-02	-
	20	4.66E-02	1.03	4.61E-03	2.20	1.8E-02	1.08	6.98E-03	1.99
	40	2.30E-02	1.02	1.08E-03	2.09	8.66E-03	1.10	1.64E-03	2.10
	80	1.14E-02	1.01	2.63E-04	2.04	4.24E-03	1.03	3.91E-04	2.06
	160	5.67E-03	1.00	6.49E-05	2.02	2.13E-03	0.99	9.52E-05	2.04
2	10	1.29E-03	-	9.37E-04	-	2.26E-03	-	1.87E-03	-
	20	1.60E-04	3.01	1.14E-04	3.04	3.56E-04	2.67	1.76E-04	3.41
	40	1.99E-05	3.00	1.41E-05	3.01	5.63E-05	2.66	2.00E-05	3.14
	80	2.49E-06	3.00	1.76E-06	3.00	9.26E-06	2.60	2.46E-06	3.03
	160	3.12E-07	3.00	2.20E-07	3.00	1.57E-06	2.56	3.06E-07	3.00

TABLE 3. Example 6.2: $\xi_0 = 0.1$ and $\xi_0 = \sqrt{3}/3$ with Neumann boundary condition.

k	N	L-mesh				C-mesh			
		$\xi_0 = 0.1$		$\xi_0 = \sqrt{3}/3$		$\xi_0 = 0.1$		$\xi_0 = \sqrt{3}/3$	
		L^2 norm	order	L^2 norm	order	L^2 norm	order	L^2 norm	order
1	10	4.18E-02	-	1.87E-02	-	4.09E-02	-	3.08E-02	-
	20	9.24E-03	2.18	4.05E-03	2.09	1.71E-02	1.26	6.99E-03	2.14
	40	2.25E-03	2.04	1.05E-03	2.07	7.31E-03	1.22	1.62E-03	2.11
	80	5.65E-04	1.99	2.55E-04	2.04	2.21E-03	1.72	3.87E-04	2.06
	160	1.42E-04	1.99	6.28E-05	2.02	5.66E-04	1.98	9.45E-05	2.03
2	10	1.51E-03	-	1.29E-03	-	2.29E-03	-	2.76E-03	-
	20	1.79E-04	3.07	1.55E-04	3.05	6.59E-04	2.68	4.60E-04	2.59
	40	2.22E-05	3.02	1.93E-05	3.01	5.65E-05	2.67	7.73E-05	2.57
	80	2.76E-06	3.00	2.41E-06	3.00	9.26E-06	2.61	1.33E-06	2.54
	160	3.45E-07	3.00	3.01E-07	3.00	1.57E-06	2.56	2.30E-06	2.52

subject to Dirichlet boundary condition

$$u(0,t) = u(2\pi,t) = 0. \tag{44}$$

Clearly, the exact solution is

$$u(x,t) = e^{-t}\sin(x).$$

We also consider a uniform mesh and take $\xi_0 = 0$ in (4). Then, we choose $\alpha = 0$, and take $\xi_0 = 0.1$ which is closed to 0 and $\xi_0 = \sqrt{3}/3$ which is away from 0. According to Table 4 and Table 5, we can observe the same outcomes discussed for the Neumann boundary condition in Example 6.2. However, we can obtain the optimal accuracy when we consider this case without the penalty term.

Example 6.4. *We solve the following heat equation in two space dimension*

$$\begin{cases} u_t = u_{xx} + u_{yy}, \quad (x,y) \in [0,2\pi] \times [0,2\pi], \\ u(x,y,0) = \cos(x)\cos(y), \end{cases} \tag{45}$$

TABLE 4. Example 6.3 midpoint with Dirichlet boundary condition.

k	N	L-mesh				C-mesh			
		no penalty		$\alpha = 1.0$		no penalty		$\alpha = 1.0$	
		L^2 norm	order	L^2 norm	order	L^2 norm	order	L^2 norm	order
1	10	7.19E-02	-	1.82E-02	-	5.04E-02	-	3.16E-02	-
	20	3.54E-02	1.02	4.26E-03	2.10	2.21E-02	1.29	6.45E-03	2.30
	40	1.76E-02	1.00	1.04E-03	2.04	9.51E-03	1.22	1.50E-03	2.10
	80	8.81E-03	1.00	2.57E-04	2.01	4.50E-03	1.08	3.70E-04	2.02
	160	4.40E-03	1.00	6.42E-05	2.00	2.18E-03	1.04	9.23E-05	2.00
2	10	1.32E-03	-	9.75E-04	-	1.96E-03	-	1.59E-03	-
	20	1.63E-04	3.01	1.16E-04	3.08	2.41E-04	3.03	2.03E-04	2.97
	40	2.02E-05	3.01	1.42E-05	3.03	2.99E-05	3.01	2.30E-05	3.14
	80	2.51E-06	3.01	1.76E-06	3.01	3.73E-06	3.00	2.68E-06	3.10
	160	3.13E-07	3.00	2.20E-07	3.00	4.66E-07	3.00	3.20E-07	3.06

TABLE 5. Example 6.3 $\xi_0 = 0.1$, and $\xi_0 = \sqrt{3}/3$ with Dirichlet boundary condition.

k	N	L-mesh				C-mesh			
		$\xi_0 = 0.1$		$\xi_0 = \sqrt{3}/3$		$\xi_0 = 0.1$		$\xi_0 = \sqrt{3}/3$	
		L^2 norm	order	L^2 norm	order	L^2 norm	order	L^2 norm	order
1	10	3.85E-02	-	1.58E-02	-	5.34E-02	-	3.91E-02	-
	20	9.56E-03	2.01	3.95E-03	2.00	2.21E-02	1.27	1.26E-02	1.63
	40	2.33E-03	2.04	9.88E-04	2.00	8.97E-03	1.30	4.02E-03	1.65
	80	5.77E-04	2.01	2.47E-04	2.00	2.73E-03	1.71	1.37E-03	1.55
	160	1.44E-04	2.00	6.18E-05	2.00	7.52E-04	1.86	4.74E-04	1.53
2	10	1.61E-03	-	1.36E-03	-	1.99E-03	-	2.30E-03	-
	20	1.87E-04	3.11	1.61E-04	3.08	2.46E-04	3.02	2.61E-04	3.14
	40	2.27E-05	3.04	1.96E-05	3.03	3.05E-05	3.01	3.07E-05	3.09
	80	2.80E-06	3.02	2.43E-06	3.01	3.81E-06	3.00	3.71E-06	3.04
	160	3.47E-07	3.01	3.02E-07	3.01	4.76E-07	3.00	4.57E-07	3.02

subject to Neumann boundary condition

$$u_x(0,y,t) = u_x(2\pi,y,t) = 0 \text{ and } u_y(x,0,t) = u_y(x,2\pi,t) = 0. \tag{46}$$

Clearly, the exact solution is

$$u(x,y,t) = e^{-2t}\cos(x)\cos(y).$$

We also consider a uniform mesh, and take $\xi_0 = 0$ and $\eta_0 = 0$ to examine the dual meshes which were generated by the midpoint in both directions. We choose the final time to be $T = 0.1$. Table 6 shows suboptimal accuracy if k is an odd number with the penalty parameter $\alpha = 0$. Also, one way to obtain the optimal accuracy is choosing $\alpha \neq 0$. However, when the C-mesh was used we can only obtain the $k + \frac{1}{2}$ order of accuracy.

Moreover, we take $\alpha = 0$, and consider the combination of $\xi_0 = 0, 0.5$ and $\eta_0 = 0, 0.5$ The results in Table 7 demonstrated that we may recover optimal

TABLE 6. Example 6.4: midpoint with Neumann boundary condition.

k	N	L-mesh				C-mesh			
		no penalty		$\alpha = 1.0$		no penalty		$\alpha = 1.0$	
		L^2 norm	order	L^2 norm	order	L^2 norm	order	L^2 norm	order
1	16	3.72E-01	-	1.34E-01	-	5.51E-01	-	5.52E-01	-
	64	1.36E-01	1.45	3.98E-02	1.78	1.92E-01	1.52	1.96E-01	1.50
	256	5.51E-02	1.30	1.12E-02	1.83	6.99E-02	1.45	6.14E-02	1.67
	1024	2.54E-02	1.11	2.81E-03	2.00	2.17E-02	1.69	2.00E-02	1.62
2	16	2.06E-01	-	2.26E-01	-	7.85E-01	-	6.23E-01	-
	64	3.40E-02	2.59	4.51E-02	2.34	1.44E-01	2.39	1.12E-01	2.47
	256	5.20E-03	2.71	7.91E-03	2.51	2.59E-02	2.48	2.02E-02	2.48
	1024	7.51E-04	2.79	1.14E-03	2.79	4.63E-03	2.48	3.65E-03	2.47
	4096	9.52E-05	2.97	1.58E-04	2.85	8.21E-04	2.49	6.54E-04	2.48
	16384	1.19E-05	2.99	1.98E-05	2.99	1.47E-04	2.49	1.18E-04	2.48

TABLE 7. Example 6.4: combination of $\xi_0 = 0, 0.5$ and $\eta_0 = 0, 0.5$ with Neumann boundary condition on L-mesh.

k	N	L-mesh					
		$\xi_0 = 0$, $\eta_0 = 0.5$		$\xi_0 = 0.5$, $\eta_0 = 0$		$\xi_0 = 0.5$, $\eta_0 = 0.5$	
		L^2 norm	order	L^2 norm	order	L^2 norm	order
1	16	3.48E-01	-	3.47E-01	-	3.22E-01	-
	64	1.15E-01	1.59	1.16E-01	1.57	9.04E-02	1.83
	256	4.22E-02	1.44	4.27E-02	1.45	2.28E-02	1.99
	1024	1.84E-02	1.19	1.85E-02	1.20	5.55E-03	2.04
2	16	1.76E-01	-	1.78E-01	-	1.69E-01	-
	64	3.76E-02	2.66	2.78E-02	2.68	2.92E-02	2.53
	256	3.74E-03	2.88	4.06E-03	2.78	4.63E-03	2.66
	1024	5.03E-04	2.90	5.78E-04	2.81	5.93E-04	2.96
	4096	6.35E-05	2.98	7.35E-05	2.98	7.59E-05	2.97
	16384	7.99E-06	2.99	9.29E-06	2.99	9.52E-06	2.99

convergence rates we if take $\xi_0 \neq 0$ and $\eta_0 \neq 0$. However, when we use the C-mesh, we can only obtain $(k + \frac{1}{2})th$ order of accuracy as shown in Table 8.

Example 6.5. *We solve*

$$\begin{cases} u_t = u_{xx} + u_{yy}, \quad (x, y) \in [0, 2\pi] \times [0, 2\pi], \\ u(x, y, 0) = \sin(x)\sin(y), \end{cases} \tag{47}$$

subject to Dirichlet boundary condition

$$u(0, y, t) = u(2\pi, y, t) = 0 \text{ and } u(x, 0, t) = u(x, 2\pi, t) = 0. \tag{48}$$

Clearly, the exact solution is

$$u(x, y, t) = e^{-2t}\sin(x)\sin(y).$$

We also explore the problem on a uniform mesh and take $\xi_0 = 0$ and $\eta_0 = 0$ to examine the dual meshes that were generated by the midpoint in both directions. We take $\alpha = 0$ and consider the combination of $\xi_0 = 0, 0.5$ and $\eta_0 = 0, 0.5$. As

TABLE 8. Example 6.4: combination of $\xi_0 = 0, 0.5$ and $\eta_0 = 0, 0.5$ with Neumann boundary condition on C-mesh.

k	N	C-mesh					
		$\xi_0 = 0$, $\eta_0 = 0.5$		$\xi_0 = 0.5$, $\eta_0 = 0$		$\xi_0 = 0.5$, $\eta_0 = 0.5$	
		L^2 norm	order	L^2 norm	order	L^2 norm	order
1	16	5.54E-01	-	5.56E-01	-	5.57E-01	-
	64	1.94E-01	1.51	1.93E-01	1.53	1.84E-02	1.60
	256	6.13E-02	1.66	5.70E-02	1.76	5.97E-02	1.62
	1024	1.99E-02	1.62	1.83E-02	1.64	1.89E-03	1.66
2	16	5.48E-01	-	4.85E-01	-	3.53E-01	-
	64	8.88E-02	2.62	7.85E-02	2.63	5.42E-02	2.70
	256	1.49E-02	2.57	1.25E-02	2.65	8.57E-02	2.66
	1024	2.59E-03	2.53	2.06E-03	2.60	1.46E-03	2.56
	4096	4.48E-04	2.53	3.45E-04	2.58	2.58E-04	2.50
	16384	8.02E-05	2.48	6.10E-05	2.50	4.57E-05	2.50

TABLE 9. Example 6.5: midpoint with Dirichlet boundary condition.

k	N	L-mesh				C-mesh			
		no penalty		$\alpha = 1.0$		no penalty		$\alpha = 1.0$	
		L^2 norm	order	L^2 norm	order	L^2 norm	order	L^2 norm	order
1	16	3.55E-01	-	8.83E-02	-	6.62E-01	-	6.63E-01	-
	64	1.08E-01	1.73	2.18E-02	2.01	18.2E-01	1.86	1.84E-01	1.85
	256	4.33E-02	1.30	5.38E-03	2.01	4.93E-02	1.86	5.20E-02	1.82
	1024	2.05E-02	1.08	1.33E-03	2.01	1.57E-02	1.64	1.45E-02	1.85
2	16	5.12E-02	-	1.69E-01	-	6.17E-01	-	5.29E-01	-
	64	9.81E-03	2.39	3.24E-02	2.39	1.27E-01	2.28	1.10E-01	2.27
	256	1.58E-03	2.63	5.37E-03	2.59	2.22E-02	2.51	1.97E-02	2.48
	1024	2.25E-04	2.81	8.54E-04	2.65	3.82E-03	2.54	3.45E-03	2.51
	4096	3.00E-05	2.90	1.07E-04	2.99	6.65E-04	2.52	6.07E-04	2.51
	16384	3.75E-06	3.00	1.34E-05	2.99	1.17E-04	2.51	1.07E-04	2.50

stated in Table 9, Table 10 and Table 11, we can observe the same results discussed for problems with Neumann boundary condition in Example 6.4.

6.2. Convection-diffusion equations. In this section, we proceed to convection-diffusion equations. For simplicity, we consider problems with both Dirichlet and Neumann boundary conditions on uniform meshes and the initial condition, Dirichlet and Neumann boundary conditions are determined by the exact solutions. Moreover, we only use the midpoint to generate the dual mesh and test the accuracy. Since the convection term may provide some numerical dissipation, we choose the penalty parameter to be zero in all the numerical examples.

Example 6.6. *We solve the following convection-diffusion equation*

$$u_t + u_x = u_{xx}, \quad x \in [0, 2\pi]. \tag{49}$$

The exact solution of this problem is

$$u(x,t) = e^{-2t}\sin(x-t). \tag{50}$$

TABLE 10. Example 6.5: combination of $\xi_0 = 0, 0.5$ and $\eta_0 = 0, 0.5$ with Dirichlet boundary condition on L-mesh.

k	N	L-mesh					
		$\xi_0 = 0$, $\eta_0 = 0.5$		$\xi_0 = 0.5$, $\eta_0 = 0$		$\xi_0 = 0.5$, $\eta_0 = 0.5$	
		L^2 norm	order	L^2 norm	order	L^2 norm	order
1	16	3.51E-01	-	3.54E-01	-	3.47E-01	-
	64	9.62E-01	1.86	1.07E-01	1.72	8.04E-02	2.05
	256	3.40E-02	1.50	4.27E-02	1.33	2.09E-02	2.01
	1024	1.49E-02	1.18	1.69E-02	1.33	5.23E-03	2.00
2	16	5.20E-02	-	5.20E-02	-	5.30E-02	-
	64	9.66E-03	2.42	9.66E-03	2.43	9.54E-03	2.47
	256	1.54E-03	2.64	1.54E-03	2.65	1.50E-03	2.67
	1024	2.12E-04	2.85	2.12E-04	2.86	1.99E-04	2.91
	4096	2.79E-05	2.93	2.79E-05	2.93	2.56E-05	2.96
	16384	3.50E-06	2.99	3.49E-06	3.00	3.20E-06	3.00

TABLE 11. Example 6.5: combination of $\xi_0 = 0, 0.5$ and $\eta_0 = 0, 0.5$ with Dirichlet boundary condition on C-mesh.

k	N	C-mesh					
		$\xi_0 = 0$, $\eta_0 = 0.5$		$\xi_0 = 0.5$, $\eta_0 = 0$		$\xi_0 = 0.5$, $\eta_0 = 0.5$	
		L^2 norm	order	L^2 norm	order	L^2 norm	order
1	16	6.62E-01	-	6.62E-01	-	6.62E-01	-
	64	1.81E-01	1.86	1.81E-01	1.87	1.80E-02	1.88
	256	4.91E-02	1.88	4.81E-02	1.91	4.77E-02	1.92
	1024	1.59E-02	1.62	1.32E-02	1.87	1.28E-03	1.91
2	16	6.48E-01	-	5.81E-01	-	6.14E-01	-
	64	1.31E-01	2.30	1.12E-01	2.37	1.17E-01	2.39
	256	2.34E-02	2.50	1.85E-02	2.60	1.96E-02	2.58
	1024	4.07E-03	2.53	3.03E-03	2.60	3.24E-03	2.60
	4096	7.10E-04	2.52	5.12E-04	2.57	5.48E-04	2.56
	16384	1.25E-05	2.51	8.83E-05	2.54	9.45E-05	2.54

We use upwind fluxes for the convection term. From Table 12, we can observe optimal convergence rates when $k = 1$. However, when we use C-mesh, we can only obtain the $(k + \frac{1}{2})$th order of accuracy if $k = 2$.

Example 6.7. *We solve the following convection-diffusion equation*

$$u_t + (\frac{u^2}{2})_x = u_{xx}, \quad x \in [0, 2\pi]. \tag{51}$$

The exact solution of this problem is

$$u(x,t) = 1 - \tanh(\frac{1}{2}(x-t)). \tag{52}$$

We use Lax-Friedrichs fluxes for the convection term and the results are given in Table 13. We can observe optimal convergence rates.

TABLE 12. Example 6.6: midpoint with Dirichlet and Neumann boundary conditions.

k	N	L-mesh				C-mesh			
		Dirichlet		Neumann		Dirichlet		Neumann	
		L^2 norm	order	L^2 norm	order	L^2 norm	order	L^2 norm	order
1	10	2.71E-02	-	2.67E-02	-	2.59E-02	-	3.91E-02	-
	20	6.73E-03	2.01	6.69E-03	2.00	6.52E-03	1.99	1.23E-02	1.67
	40	1.66E-03	2.01	1.63E-03	2.03	1.64E-03	1.99	3.47E-03	1.83
	80	4.16E-04	2.00	3.99E-04	2.03	4.12E-04	1.99	8.98E-04	1.95
	160	1.05E-04	2.00	9.85E-05	2.02	1.04E-04	1.99	2.27E-04	1.98
2	10	1.62E-03	-	1.40E-03	-	2.16E-03	-	1.94E-03	-
	20	2.41E-04	2.75	1.75E-04	3.00	3.47E-04	2.63	2.56E-04	2.92
	40	3.22E-05	2.90	2.34E-05	2.91	6.19E-05	2.49	3.73E-05	2.77
	80	4.28E-06	2.91	2.98E-06	2.98	1.09E-05	2.51	6.77E-06	2.46
	160	5.47E-07	2.97	3.75E-07	2.99	1.91E-06	2.51	1.19E-06	2.50

TABLE 13. Example 6.7: midpoint with Dirichlet and Neumann boundary conditions.

k	N	L-mesh				C-mesh			
		Dirichlet		Neumann		Dirichlet		Neumann	
		L^2 norm	order	L^2 norm	order	L^2 norm	order	L^2 norm	order
1	10	3.80E-03	-	3.79E-03	-	3.82E-03	-	3.78E-03	-
	20	9.52E-04	1.99	9.50E-04	1.99	9.52E-04	2.00	6.49E-04	1.99
	40	2.38E-04	2.00	2.38E-04	2.00	2.38E-04	2.00	2.38E-04	2.00
	80	5.95E-05	2.00	5.98E-05	2.00	5.94E-05	2.00	3.00E-05	1.99
	160	1.49E-05	2.00	1.52E-05	1.99	1.48E-05	2.00	1.53E-05	1.97
2	10	3.30E-04	-	1.70E-04	-	5.90E-04	-	2.47E-04	-
	20	4.60E-05	2.84	2.20E-05	2.95	7.42E-05	2.99	3.36E-05	2.87
	40	6.17E-06	2.90	3.10E-06	2.82	9.31E-06	2.99	4.45E-06	2.92
	80	7.92E-07	2.96	4.82E-07	2.69	1.17E-06	2.99	5.58E-07	3.00
	160	9.92E-08	3.00	6.32E-08	2.93	1.47E-07	3.00	7.09E-08	2.98

Example 6.8. *We solve the following convection-diffusion equation in two space dimensions*

$$u_t + u_x + u_y = u_{xx}, \quad (x, y) \in [0, 2\pi] \times [0, 2\pi]. \tag{53}$$

The exact solution of this problem is

$$u(x, y, t) = e^{-2t} \sin(x - t) sin(y - t). \tag{54}$$

We use upwind fluxes for the convection term and the results are given in Table 14. Different from the 1D case, we can observe optimal convergence rates.

Example 6.9. *We solve the following nonlinear convection-diffusion equation in two space dimensions*

$$u_t + (\frac{u^2}{2})_x + (\frac{u^2}{2})_y = u_{xx} + u_{yy}, \quad (x, y) \in [0, 2\pi] \times [0, 2\pi]. \tag{55}$$

TABLE 14. Example 6.8: midpoint with Dirichlet and Neumann boundary conditions.

k	N	L-mesh				C-mesh			
		Dirichlet		Neumann		Dirichlet		Neumann	
		L^2 norm	order	L^2 norm	order	L^2 norm	order	L^2 norm	order
1	16	6.66E-01	-	6.86E-01	-	6.79E-01	-	6.91E-01	-
	64	1.85E-01	1.84	1.86E-01	1.88	1.31E-01	1.83	1.86E-01	1.89
	256	4.76E-02	1.96	4.75E-02	1.97	4.88E-02	1.97	4.76E-02	1.97
	1024	1.20E-03	1.99	1.19E-02	1.99	1.22E-03	2.00	1.20E-02	1.99
	4096	2.99E-04	1.99	2.98E-03	2.00	3.05E-03	2.00	3.02E-03	1.99
2	16	1.76E-01	-	2.19E-01	-	2.51E-01	-	1.94E-01	-
	64	2.36E-02	2.90	2.95E-02	2.89	3.25E-02	2.95	3.25E-02	2.58
	256	3.00E-03	2.97	3.97E-03	2.90	4.19E-03	2.96	4.96E-03	2.71
	1024	3.77E-04	2.99	4.99E-04	2.99	5.39E-04	2.96	6.55E-04	2.92
	4096	4.78E-05	2.98	6.34E-05	2.98	6.79E-05	2.99	8.31E-05	2.98

TABLE 15. Example 6.9: midpoint with Dirichlet and Neumann boundary conditions.

k	N	L-mesh				C-mesh			
		Dirichlet		Neumann		Dirichlet		Neumann	
		L^2 norm	order	L^2 norm	order	L^2 norm	order	L^2 norm	order
1	16	4.87E-02	-	6.87E-01	-	4.86E-02	-	7.03E-02	-
	64	1.29E-02	1.91	1.86E-01	1.88	1.29E-02	1.91	2.04E-02	1.61
	256	3.27E-03	1.98	4.76E-02	1.97	3.27E-03	1.98	7.12E-03	1.75
	1024	8.19E-04	2.00	1.20E-02	1.99	8.19E-04	2.00	1.96E-04	1.85
	4096	2.05E-04	2.00	3.02E-03	1.99	2.05E-04	2.00	5.04E-04	1.96
2	16	8.21E-03	-	1.41E-02	-	9.63E-03	-	8.90E-03	-
	64	1.02E-03	3.00	1.97E-03	2.84	1.25E-03	2.94	1.19E-03	2.90
	256	1.29E-04	2.98	2.56E-04	2.94	1.59E-04	2.97	1.54E-04	2.95
	1024	1.64E-05	2.98	3.25E-05	2.98	2.01E-05	2.98	1.96E-05	2.97
	4096	2.08E-06	2.98	4.07E-06	2.99	2.53E-06	2.99	2.49E-06	2.98

The exact solution of this problem is

$$u(x,t) = 1 - \tanh(\frac{1}{2}(x+y+1) - t). \tag{56}$$

We also use Lax-Friedrichs fluxes for the convection term and the results are given in Table 15. We can also observe optimal convergence rates.

7. Conclusion

In this paper, we demonstrate the algorithms of the LDG method on overlapping mesh for Neumann and Dirichlet boundary conditions. The scheme for each boundary condition is stable with adjusted boundary cells but the order of accuracy may not be optimal. We observed that C-mesh could yield larger time step than L-mesh. However, in some cases, C-mesh cannot yield optimal convergence rates. With a positive penalty parameter, L-meshes can result in optimal convergence rates.

Acknowledgements

This work is supported by NSF grant DMS-1818467 and KMITL Research Fund, Research Seed Grant for New Lecturer.

References

[1] F. Bassi, S. Rebay, A high-order accurate discontinuous finite element method for the numerical solution of the compressible Navier-Stokes equations, Journal of Computational Physics, 131 (1997), 267-279.
[2] N. Chuenjarern, Z. Xu and Y. Yang, High-order bound-preserving discontinuous Galerkin methods for compressible miscible displacements in porous media on triangular meshes, Journal of Computational Physics, 378 (2019), 110-128.
[3] N. Chuenjarern, Y. Yang, Fourier analysis of local discontinuous Galerkin method for linear parabolic equations on overlapping meshes, Journal of Scientific Computing, 81 (2019), 671-688.
[4] E. Chung and C.S. Lee, A staggered discontinuous Galerkin method for convection-diffusion equations, Journal of Numerical Mathematics, 20 (2012), 1-31.
[5] P.G. Ciarlet, Finite element method for elliptic problems, North-Holland, Amsterda, 1978.
[6] B. Cockburn, S. Hou, C. W. Shu, The Runge-Kutta local projection discontinuous Galerkin finite element method for conservation laws. IV: The multidimensional case, Mathematics Computation, 54 (1990), 545-581.
[7] B. Cockburn, S. Y. Lin, C. W. Shu, TVB Runge-Kutta local projection discontinuous Galerkin finite element method for conservation laws. III: One-dimensional systems, Journal of Computational Physics, 84 (1989), 90-113.
[8] B. Cockburn, C. W. Shu, TVB Runge-Kutta local projection discontinuous Galerkin finite element method for conservation laws. II: General framework, Mathematics Computation, 52 (1989), 411-435.
[9] B. Cockburn, C. W. Shu, The Runge-Kutta discontinuous Galerkin method for conservation laws. V: Multidimensional systems, Journal of Computational Physics, 141 (1998), 199-224.
[10] B. Cockburn, C.-W. Shu, The local discontinuous Galerkin method for time-dependent convection-diffusion systems, SIAM Journal on Numerical Analysis, 35 (1998), 2440-2463.
[11] J. Douglas, Jr., R.E. Ewing and M.F. Wheeler, phA time-discretization procedure for a mixed finite element approximation of miscible displacement in porous media, R.A.I.R.O. Analyse numérique, 17 (1983), 249-256.
[12] J. Douglas, Jr., R.E. Ewing and M.F. Wheeler, phThe approximation of the pressure by a mixed method in the simulation of miscible displacement, R.A.I.R.O. Analyse numérique, 17 (1983), 17-33.
[13] J. Du and Y. Yang, Maximum-principle-preserving third-order local discontinuous Galerkin methods on overlapping meshes, Journal of computational physics, 377 (2019), 117-141.
[14] J. Du, Y. Yang and E. Chung, Stability analysis and error estimates of local discontinuous Galerkin method for convection-diffusion equations on overlapping meshes, BIT Numerical Mathematics, 59 (2019), 853-876.
[15] S. Gottlieb, C.-W. Shu and E. Tadmor, Strong stability-preserving high-order time discretization method, SIAM Review, 43(2001), 89-112.
[16] H. Guo, F. Yu and Y. Yang, Local discontinuous Galerkin method for incompressible miscible displacement problem in porous media, Journal of Scientific Computing, 71 (2017), 615-633.
[17] H. Guo and Y. Yang, Bound-preserving discontinuous Galerkin method for compressible miscible displacement problem in porous media, SIAM Journal on Scientific Computing, 39 (2017), A1969-A1990.
[18] H. Guo, Q. Zhang and Y. Yang, A combined mixed finite element method and local discontinuous Galerkin method for miscible displacement problem in porous media, Science China Mathematics, 57 (2014), 2301-2320.
[19] E. F. Keller and L. A. Segal, Initiation on slime mold aggregation viewed as instability, Journal of Theoretical of Biology, 26 (1970), 399-415
[20] X. Li, C.-W. Shu and Y. Yang, Local discontinuous Galerkin method for the Keller-Segel chemotaxis model, Journal of Scientific Computing, 73 (2017), 943-967.
[21] Y. Liu, C.-W. Shu, E. Tadmor and M. Zhang, Central local discontinuous Galerkin method on overlapping cells for diffusion equations, ESAIM: Mathematical Modelling and Numerical Analysis (M2AN), 45 (2011), 1009-1032.

[22] C. Patlak, Random walk with persistence and external bias, The bulletin of mathematical biophysics, 15 (1953), 311-338.
[23] W.H. Reed and T. R. Hill, Triangular mesh method for the neutron transport equation, Los Alamos Scientific Laboratory Report LA-UR-73-479, Los Alamos, NM, 1973.
[24] H. Wang, C.-W. Shu, and Q. Zhang, Stability and error estimates of local discontinuous Galerkin methods with implicit-explicit time-marching for advection-diffusion problems, SIAM Journal on Numerical Analysis, 53 (2015), 206-227.
[25] H. Wang, C.-W. Shu and Q. Zhang, Stability analysis and error estimates of local discontinuous Galerkin methods with implicit-explicit time-marching for nonlinear convection-diffusion problems, Applied Mathematics and Computation, 272 (2016), 237-258.
[26] H. Wang, S. Wang, Q. Zhang and C.-W. Shu, Local discontinuous Galerkin methods with implicit-explicit time marching for multi-dimensional convection diffusion problems, ESAIM:M2AN, 50 (2016), 1083-1105.
[27] T. Xiong, J.-M. Qiu and Z. Xu, High order maximum-principle-preserving discontinuous Galerkin method for convection-diffusion equations, SIAM Journal on Scientific Computing, 37 (2015), A583-A608.
[28] F. Yu, H. Guo, N. Chuenjarern and Y. Yang, Conservative local discontinuous Galerkin method for compressible miscible displacements in porous media, Journal of Scientific Computing, 73 (2017), 1249-1275.
[29] M. Zhang and C.-W. Shu, An analysis of three different formulations of the discontinuous Galerkin method for diffusion equations, Mathematical Models and Methods in Applied Sciences, 13 (2003), 395-413.

Department of Mathematics, King Mongkut's Institute of Technology Ladkrabang, Bangkok 10520, Thailand
E-mail: nattaporn.ch@kmitl.ac.th and kanognudge.wu@kmitl.ac.th

Department of Mathematical Sciences, Michigan Technological University Houghton, MI 49931, USA
E-mail: yyang7@mtu.edu